

Article

Fe-mediated HER vs N₂RR: Exploring Factors that Contribute to Selectivity in P₃EFe(N₂-) (E = B, Si, C) Catalyst Model Systems

Benjamin D. Matson, and Jonas C. Peters

ACS Catal., Just Accepted Manuscript • DOI: 10.1021/acscatal.7b03068 • Publication Date (Web): 03 Jan 2018

Downloaded from <http://pubs.acs.org> on January 4, 2018**Just Accepted**

“Just Accepted” manuscripts have been peer-reviewed and accepted for publication. They are posted online prior to technical editing, formatting for publication and author proofing. The American Chemical Society provides “Just Accepted” as a free service to the research community to expedite the dissemination of scientific material as soon as possible after acceptance. “Just Accepted” manuscripts appear in full in PDF format accompanied by an HTML abstract. “Just Accepted” manuscripts have been fully peer reviewed, but should not be considered the official version of record. They are accessible to all readers and citable by the Digital Object Identifier (DOI®). “Just Accepted” is an optional service offered to authors. Therefore, the “Just Accepted” Web site may not include all articles that will be published in the journal. After a manuscript is technically edited and formatted, it will be removed from the “Just Accepted” Web site and published as an ASAP article. Note that technical editing may introduce minor changes to the manuscript text and/or graphics which could affect content, and all legal disclaimers and ethical guidelines that apply to the journal pertain. ACS cannot be held responsible for errors or consequences arising from the use of information contained in these “Just Accepted” manuscripts.

Fe-mediated HER vs N₂RR: Exploring Factors that Contribute to Selectivity in P₃^EFe(N₂) (E = B, Si, C) Catalyst Model Systems

Benjamin D. Matson and Jonas C. Peters*

Division of Chemistry and Chemical Engineering, California Institute of Technology (Caltech), Pasadena, California 91125, United States

Abstract: Mitigation of the hydrogen evolution reaction (HER) is a key challenge in selective small molecule reduction catalysis. This is especially true of catalytic nitrogen (N₂) and carbon dioxide (CO₂) reduction reactions (N₂RR and CO₂RR, respectively) using H⁺/e⁻ currency. Here we explore, via DFT calculations, three iron model systems, P₃^EFe (E = B, Si, C), known to mediate both N₂RR and HER, but with different selectivity depending on the identity of the auxiliary ligand. It is suggested that the respective efficiencies of these systems for N₂RR trend with the predicted N–H bonds strengths of two putative hydrazido intermediates of the proposed catalytic cycle, P₃^EFe(NNH₂)⁺ and P₃^EFe(NNH₂). Further, a mechanism is presented for undesired HER consistent with DFT studies, and previously reported experimental data, for these systems; bimolecular proton-coupled-electron-transfer (PCET) from intermediates with weak N–H bonds is posited as an important source of H₂ instead of more traditional scenarios that proceed via metal hydride intermediates and proton transfer/electron transfer (PT/ET) pathways. Wiberg bond indices provide additional insight into key factors related to the degree of stabilization of P₃^EFe(NNH₂) species, factors that trend with overall product selectivity.

KEYWORDS: nitrogen fixation, N₂RR, HER, hydrogen evolution, PCET, HAT, nitrogenase

Introduction

The reduction of nitrogen (N₂) to ammonia (NH₃) by nitrogenase enzymes (the nitrogen reduction reaction: N₂RR) has garnered substantial interest in the synthetic inorganic community for several decades.¹ In particular, the structural characterization of the FeMo-cofactor active site of biological nitrogen fixation,² and mechanistic uncertainties associated with this process,³ have motivated studies of synthetic (primarily Mo and Fe) model systems that mediate N₂RR in the presence of proton and electron equivalents in organic solvent.⁴⁻⁶ The mechanisms of these systems are at various stages of understanding. Experimental^{4, 5, 6} and theoretical (predominantly Mo)⁷ studies have been undertaken to provide insight.

Single-site iron model complexes, such as P₃^BFe(N₂)⁻ and P₃^BFe⁺ (**Figure 1**), catalyze N₂RR under a variety of conditions and driving forces, with reported selectivities (to date) for NH₃ generation as high as 72% based on reductant consumed.^{4e} In addition, conditions have been reported under which P₃^CFe(N₂)⁻ and P₃^{Si}Fe(N₂)⁻ also catalyze N₂RR to varying degrees, with the P₃^{Si}Fe-system being far more efficient at the hydrogen evolution reaction (HER) than N₂RR compared to

P₃^BFe and P₃^CFe.^{4d,8} We are naturally interested in understanding the mechanism/s by which catalysis in these respective systems occurs, and in exploring alternative systems that might function similarly. Of interest to the present study is the interplay between efficiency for the N₂RR and HER on the P₃^BFe scaffold and its isostructural congeners P₃^{Si}Fe and P₃^CFe. In particular, can we elucidate some of the salient factors that dictate overall product selectivity for NH₃ versus H₂ in these respective systems?

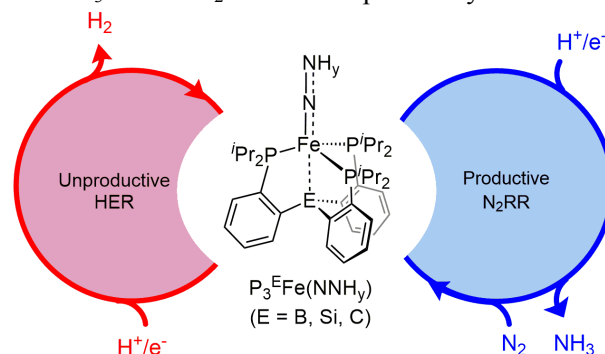


Figure 1. Schematic depiction of N₂RR/HER iron catalysts studied herein to explore key factors dictating product selectivity.

Herein we use DFT calculations to explore this question. We examine the comparative

feasibility of HER via proton-coupled electron transfer (PCET)⁹ from several putative Fe(N_xH_y) early intermediates, using electronic structure calculations coupled with predicted N–H bond strengths, thermodynamic driving forces, and electron-transfer (ET) kinetics as mechanistic probes. Acknowledging the likelihood that numerous and potentially competing factors may be at play, the formation, electronic structure, and reactivity of a key common intermediate, Fe(NNH₂)⁺, is highlighted to be an important factor in the divergent selectivity profile of P₃^BFe (and P₃^CFe) relative to the P₃^{Si}Fe system.

Computational Methods

All calculations were performed using dispersion corrected density functional theory (DFT-D₃) using Grimmes dispersion correction.¹⁰ All calculations were done using the full P₃^EFe scaffold with the TPSS functional¹¹ and a def2-TZVP basis set on transition metals and a def2-SVP basis set on all other atoms.¹²

All stationary point geometries were optimized using NWChem 6.3¹³ or Orca 3.0.3.¹⁴ To ensure consistency in grid size, all reported single point and thermodynamic energies were performed using Orca 3.0.3. Frequency calculations were used to confirm the presence of true minima and to obtain gas phase free-energy values at 195 K (*G*_{gas}). Solvation corrections were performed using the COSMO-SMD continuum model.¹⁵ The solvation free energy was approximated using gas phase and solvated single point energies ($\Delta G_{\text{solv}} \approx E_{\text{soln}} - E_{\text{gas}}$). Finally, the free-energy of the solvated species at 195 K was calculated using the gas-phase free-energy and the solvation free-energy ($G_{\text{soln},195\text{K}} = G_{\text{gas},195\text{K}} + \Delta G_{\text{solv}}$).¹⁶

The accuracy of the described computational methodology was measured by comparison to several experimental benchmarks of interest. In addition to ensuring good agreement between computed and crystallographically determined structural data, experimentally determined bond dissociation enthalpies (BDFE_{N-H}) of the compounds P₃^{Si}Fe(CNH)⁺, P₃^{Si}Fe(CNH), P₃^{Si}Fe(CNMeH)⁺, P₃^{Si}Fe(CNMeH) and P₃^{Si}Fe(NNMeH)⁺ could be faithfully reproduced within ± 2 kcal/mol (See SI for full description).^{4h} As a further point of calibration, the calculated singlet-triplet energy gap and the redox potentials of P₃^BFe(NNMe₂) and P₃^{Si}Fe(NNMe₂)⁺ are in good agreement with the experimentally determined values (within ± 1.5 kcal/mol, and ± 3 kcal/mol (± 130 mV vs $\text{Fc}^{+/0}$), respectively; see SI).^{4g,h,17}

Reduction kinetics were calculated using the standard Marcus equation relating activation barrier with driving force and total reorganization energy ($\lambda_{\text{tot}} = \lambda_{\text{is}} + \lambda_{\text{os}}$).¹⁸ The inner-sphere reorganization energy for electron transfer ($\lambda_{\text{is,ET}}$) was estimated assuming non-adiabatic behavior and by calculating the difference between the single point energies of the relevant species in its ground state and the corresponding single point energy of this ground state in the oxidized or reduced geometry (Eq. 1).

$$\lambda_{\text{is,ET}} = [E(\text{Fe}^{\text{ox}}_{\text{ox}}) - E(\text{Fe}^{\text{ox}}_{\text{red}})] + [E(\text{Fe}^{\text{red}}_{\text{red}}) - E(\text{Fe}^{\text{red}}_{\text{ox}})] \quad (1)$$

The outer-sphere reorganization energy was calculated by assuming a barrier of 1.0 kcal/mol for the reduction of P₃^BFe(NNH₂)⁺ followed by calculation of λ_{tot} using this barrier and λ_{is} , as calculated by Eq 1. A continuum solvation model was used to confirm that $\lambda_{\text{os}} \approx \lambda_{\text{is}}$ (See SI for full description).¹⁸ Reduction barriers for P₃^{C/Si}Fe(NNH₂)⁺ were subsequently calculated relative to P₃^BFe(NNH₂)⁺.

Results and Discussion

To set the stage for the present study, previously reported catalytic N₂-to-NH₃ conversion studies by P₃^EFe (E = B, C, and Si) under an atmosphere of N₂ at -78 °C in Et₂O, using KC₈ and [(Et₂O)₂H][BAR^F₄] (HBAr^F₄, BAR^F₄ = tetrakis-(3,5-bis(trifluoromethyl)phenyl)borate) as the reductant and acid source,^{4a,d} established P₃^BFe as the most efficient catalyst for N₂RR; the highest reported efficiency for this system (under these conditions) was $45 \pm 3\%$ (48 equiv acid; 58 equiv reductant). For comparison, the P₃^{Si}Fe system provided a conversion efficiency of only $5 \pm 3\%$. The P₃^CFe catalyst system was reasonably active at $36 \pm 6\%$ (note: $\sim 25\%$ lower substrate loading was used for this P₃^CFe value^{4d}). Measurement of HER activity established P₃^{Si}Fe(N₂)⁻ (88% per added acid equiv) as a significantly more efficient HER catalyst than P₃^BFe(N₂)⁻ (40% per added acid equiv) under analogous conditions.^{4d} N₂RR catalysis by P₃^EFe (E = B, Si) has also been studied in the presence of milder reagents (e.g., Cp*₂Co and [H₂NPh₂][OTf] or [H₃NPh][OTf]); under these conditions only the P₃^BFe system is catalytically active.

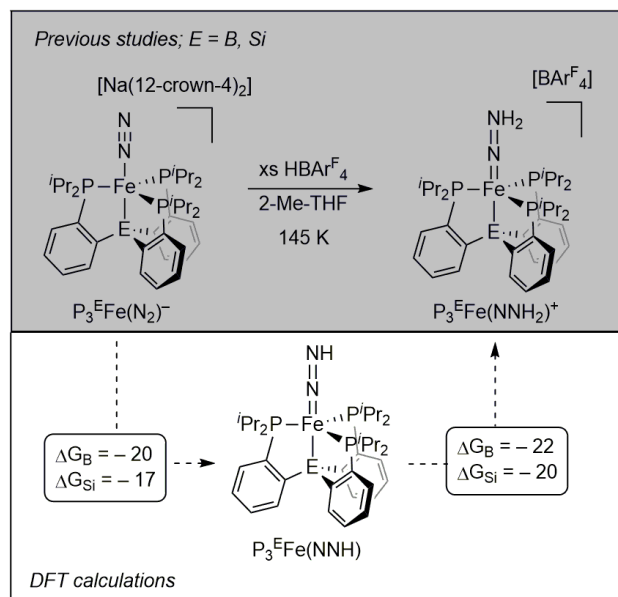


Figure 2. (top) Previous experimental work showing the formation of $\text{P}_3^{\text{E}}\text{Fe}(\text{NNH}_2)^+$ (E = B or Si) via protonation with excess acid.^{4f,g} (bottom) Calculated free energy changes (in kcal/mol; 195 K) for the formation of $\text{P}_3^{\text{E}}\text{Fe}(\text{NNH}_2)^+$ via $\text{P}_3^{\text{E}}\text{Fe}(\text{NNH})$ (E = B or Si).

Previous studies of the $\text{P}_3^{\text{B}}\text{Fe}$ and $\text{P}_3^{\text{Si}}\text{Fe}$ systems have also explored the generation and characterization of early stage intermediates of the N_2RR catalysis.^{4e,f,g} Most salient, low temperature protonation of $\text{P}_3^{\text{E}}\text{Fe}(\text{N}_2)^-$ (E = B, Si) with excess HBAR^{F}_4 affords the doubly protonated $\text{P}_3^{\text{E}}\text{Fe}(\text{NNH}_2)^+$ species (**Figure 2**).^{4f,g} As expected, corresponding DFT calculations (this work) are consistent with thermodynamically favored formation of $\text{P}_3^{\text{E}}\text{Fe}(\text{NNH})$ via proton transfer (**Figure 2**); another favorable proton transfer forms $\text{P}_3^{\text{E}}\text{Fe}(\text{NNH}_2)^+$.

DFT Support for Slow Fe Protonation and Fast $\text{Fe-N}_x\text{H}_y$ Formation

Although metal hydride (M–H) species are most typically invoked as intermediates of transition-metal catalyzed HER,¹⁹ we do not think Fe–H species are the primary players in H_2 formation by the present systems. Several experimental observations are consistent with this idea. Foremost among them is that low temperature addition of stoichiometric acid (e.g., HBAR^{F}_4) to any of the anions, $\text{P}_3^{\text{E}}\text{Fe}(\text{N}_2)^-$, causes overall oxidation to their corresponding neutral products, $\text{P}_3^{\text{E}}\text{Fe}(\text{N}_2)$, along with release of 0.5 equiv H_2 .^{4a,d} This is noteworthy because for E = Si or C the diamagnetic hydride products, $\text{P}_3^{\text{E}}\text{Fe}(\text{N}_2)(\text{H})$, are very stable species and are formed during catalysis as end

products.^{4b,d} We posit that reactive $\text{P}_3^{\text{E}}\text{Fe}(\text{N}_x\text{H}_y)$ intermediates instead undergo net bimolecular HAT reactions to liberate H_2 via N_xH_y -ligand-mediated steps (*vide infra*). While iron hydrides (Fe–H) can tie up the population of active catalyst, in our view they are unlikely to be intermediates of the dominant HER pathway.

To speak to this hypothesis computationally, we focus on one acid source, HBAR^{F}_4 , as it has been the subject of the most extensive comparative study.^{4d} The solid-state empirical formula of HBAR^{F}_4 reveals the presence of two ethers per HBAR^{F}_4 ($[(\text{Et}_2\text{O})_2\text{H}][\text{BAR}^{\text{F}}_4]$).²⁰ To determine the preferred solution-state structure of this acid, optimizations were performed in which a Et_2OH^+ species was provided with 0, 1 or 2 explicit Et_2O molecules with which to hydrogen bond. We found that $[(\text{Et}_2\text{O})_2\text{H}]^+$ speciation was lowest in free-energy, with $[(\text{Et}_2\text{O})_3\text{H}]^+$ and $[\text{Et}_2\text{OH}]^+$ higher in energy by +7.0 and +8.2 kcal/mol, respectively (see SI).

The structure of HBAR^{F}_4 is particularly crucial for Fe protonation, as a pre-equilibrium formation of the $[\text{Et}_2\text{OH}]^+$ appears to be required, as evidenced by relaxed surface scans. The need for dissociation of Et_2O prior to Fe protonation provides a lower bound on the barrier of +8.2 kcal/mol. The requirement of $[\text{Et}_2\text{OH}]^+$ as the active acid, as opposed to $[(\text{Et}_2\text{O})_2\text{H}]^+$, is presumably steric in origin and may speak, in part, to the importance of bulky isopropyl-phosphino substituents in these catalysts. Our lab recently reported that a structurally related $\text{P}_3^{\text{Si}}\text{Os}(\text{N}_2)^-$ complex is an active catalyst for N_2RR .²¹ In contrast to the $\text{P}_3^{\text{E}}\text{Fe}(\text{N}_2)^-$ catalysts, stoichiometric HBAR^{F}_4 addition can protonate at the metal, generating Os–H species that are not catalytically active for N_2RR . Steric access to the larger Os center is presumably less restricted than it is for Fe.

The steric profile of the $\text{Fe}(\text{N}_2)$ unit suggests that functionalization of the $\beta\text{-N}$ should not be subject to the same pre-equilibrium. This is consistent with relaxed surface scans, which show that the N_2 unit can be protonated in a concerted, low energy step in which an Et_2O molecule is favorably displaced by the nucleophilic $\beta\text{-N}$ -atom. Subsequent proton transfers yield $\text{Fe}(\text{NNH})$ with a low overall kinetic barrier (0.5–1.0 kcal/mol; see SI).

Fe–H formation is thermodynamically favored for all three scaffolds. We therefore presume that the dominant source of HER for these systems is not via Fe–H formation, but that hydride species are formed over the course of catalysis as thermodynamic products. We presume that both

HER and N₂RR, under the conditions explored in this work, are operating under kinetic control. In subsequent results and discussion, thermodynamics are assumed to be relevant within the context of kinetic parameters.

In addition to restricting our analysis to a single acid, HBAR^F₄, we focus on KC₈ as a reductant for several reasons. Most salient is that KC₈ is the only reductant that has been shown to produce catalytic yields of NH₃ for all scaffolds considered. This observation is attributed to the requirement of Fe(N₂)⁻ formation during catalysis. While P₃^BFe(N₂)⁻ can be formed with weaker reductants, namely Cp*₂Co, the more reducing P₃^{Si/C}Fe(N₂)⁻ is believed to be inaccessible under these conditions. Additionally, it has been noted that, when using KC₈ and HBAR^F₄, HER and N₂RR proceed with similar initial rates on P₃^{Si}Fe and P₃^BFe scaffolds,^{4d} possibly due to Fe(N₂) reduction being a common rate limiting step. Further the initial rates of N₂RR are similar between the scaffolds, which makes this reductant/acid combination well suited for a comparative study.

Despite the need to restrict the scope of this study to a specific catalysis cocktail, many of the conclusions should extend to other conditions reported for N₂RR catalysis using P₃^EFe (and related) complexes. In particular, the BDFE_{N-H} values reported herein are acid and reductant independent and hence provide insight into the anticipated stability and reactivity profiles of key early intermediates of N₂RR.

Calculation of BDFE_{N-H} Values for Fe-N_xH_y Intermediates

Early stage intermediates of the type Fe(NNH) and Fe(NNH₂) are expected to be highly reactive,^{4e,h} thermochemical calculations reveal the presence of extremely weak N-H bonds in these systems, as shown by their calculated bond dissociation enthalpies (BDFE_{N-H}; **Figure 3**). In particular, as yet unobservable P₃^EFe(NNH) intermediates are predicted to have extremely weak N-H bonds (< 40 kcal/mol), and should therefore be subject to rapid bimolecular loss of H₂ and generation of P₃^EFe(N₂). By contrast, the BDFE_{N-H} values of candidate P₃^EFe(N_xH_y) intermediates that are further downstream (e.g., Fe(N₂H₄), Fe(NH), Fe(NH₂)) are predicted to be significantly larger (**Figure 3**). This notion is consistent with the solution stability of characterized examples of such

downstream intermediates, contrasting the high degree of solution instability of earlier intermediates.

Of particular interest herein is that the BDFE_{N-H} values for the P₃^{Si}Fe(NNH₂)ⁿ⁺ (n = 0, 1) system are lower than those for P₃^{B/C}, for a given overall charge. As discussed later, these different BDFE_{N-H} values are rooted in the different valence electron counts, and hence electronic structures, of the respective P₃^EFe-systems.

For additional context, it is useful to consider reported BDFE_{N-H} data for a related P₃^{Si}Fe(CN)-system. The relevant P₃^{Si}Fe(CNH) species, isoelectronic with P₃^BFe(NNH), is calculated to have a weak BDFE_{N-H} of 43.5 kcal/mol, in close agreement to that of 41.4 kcal/mol determined experimentally.^{4h} Accordingly, P₃^{Si}Fe(CNH) loses 0.5 equiv H₂ rapidly in solution to afford P₃^{Si}Fe(CN). In contrast, its oxidized cation, P₃^{Si}Fe(CNH)⁺, has a much higher BDFE_{N-H} (61.8 kcal/mol (calc); 61.9 kcal/mol (exp)); this species is stable to H₂ loss in solution and can be isolated and structurally characterized.

Considering these collected data and observations, and additional data discussed below, we presume that the earliest N₂RR intermediates in P₃^EFe-systems are very important for determining N₂RR versus HER selectivity; they engage in bimolecular H₂-evolving reactions that compete with productive N₂RR. We next consider aspects of the H-H bond-forming steps in these early P₃^EFe(N_xH_y) intermediates in more detail.

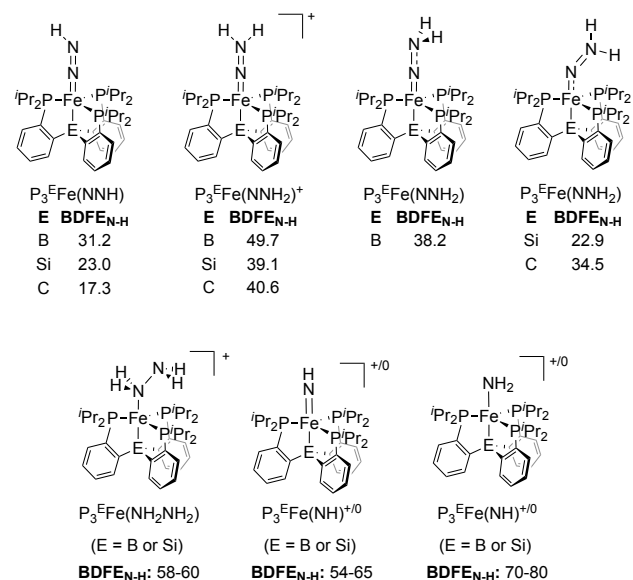


Figure 3. BDFE_{N-H} values (in kcal/mol) for selected P₃^EFe(N_xH_y) species.²²

P₃^EFe(NNH) species are plausible candidates to consider with respect to selectivity

since bimolecular H₂-evolving reactions can presumably result from their extremely weak N–H bonds (Figure 3; 31–17 kcal/mol). P₃^{Si}Fe(NNH), with a BDFE_{N–H} estimated to be 8.2 kcal/mol lower than for P₃^BFe(NNH), might be reasonably expected to liberate H₂ more readily, thereby attenuating its N₂RR efficiency. However, the BDFE_{N–H} for P₃^CFe(NNH) is calculated to be even lower (17.3 kcal/mol) than for P₃^{Si}Fe(NNH) (23 kcal/mol), despite the fact that P₃^CFe(N₂)[–] is appreciably more efficient for N₂RR. Hence, a trend is not evident on the basis of the Fe(NNH) intermediates, at least as related to their relative BDFE_{N–H} values. Fe(NNH) intermediates are readily protonated to form Fe(NNH₂)⁺ species in solution at low temperature (Figure 2). This likewise suggests that Fe(NNH) intermediates are unlikely to be primarily responsible for HER under catalytic conditions when a large excess of acid is present.^{4f,g}

P₃^EFe(NNH₂)⁺ BDFE_{N–H} values provide a more tractable trend: the respective calculated values are 38.2 kcal/mol for P₃^BFe, 34.4 kcal/mol for P₃^CFe, and 22.9 kcal/mol for P₃^{Si}Fe; the P₃^EFe–NNH₂ species that exhibits the most efficient N₂RR activity exhibits the strongest N–H bond, and the least efficient exhibits the weakest (Figure 3).

Calculated Reduction Kinetics of P₃^EFe(NNH₂)⁺

To gain further insight into the respective role P₃^EFe(NNH₂)⁺⁰ (E = B, Si, C) species might play in dictating product selectivity, P₃^EFe(NNH₂)⁺ reduction kinetics were derived using the standard Marcus equation relating the driving force and total reorganization energy with the ET activation barrier.¹⁸ Comparison of the optimized Fe(NNH₂) and Fe(NNH₂)⁺ redox pairs reveals significant differences in their respective reduction potentials and inner-sphere reorganization energies (λ_{is,ET}).

The P₃^BFe(NNH₂)⁺ species is predicted to have a considerably more positive reduction potential (–1.2 V vs Fc/Fc⁺) than P₃^{Si}Fe(NNH₂)⁺ (–1.9 V; Table 1), resulting from their different valence electronic counts and electronic structures (see below). Given their dramatic difference in reduction potentials, the barrier for reduction (G*) is expected to sharply increase in moving from B to Si. Relative reduction barrier calculations, assuming G* = 1.0 kcal/mol for the reduction of P₃^BFe(NNH₂)⁺, predict activation barriers that are 4–5 times higher in energy for the reduction of P₃^{C/Si}Fe(NNH₂)⁺ versus P₃^BFe(NNH₂)⁺ (Table 1). While the reduction of all three species should be more than readily

accomplished by the strong reductant KC₈, P₃^{C/Si}Fe(NNH₂)⁺ species are predicted to be significantly longer lived than the P₃^BFe(NNH₂)⁺ congener.

To roughly quantify the differences in reduction rate between P₃^EFe(NNH₂)⁺ species, and hence get a sense of their relative expected lifetimes, we turned to transition state theory. By assuming a pre-exponential factor invariant across both scaffolds, reduction rates for P₃^{Si}Fe(NNH₂)⁺ and P₃^CFe(NNH₂)⁺, normalized to P₃^BFe(NNH₂)⁺ (k_{rel}), were calculated (k_{rel} = 2x10^{–4} and 2x10^{–5}, respectively). Accordingly, we expect P₃^{Si}Fe(NNH₂)⁺ and P₃^CFe(NNH₂)⁺ to be ~ 10⁴ times longer-lived, respectively, than P₃^BFe(NNH₂)⁺, with respect to one-electron reduction.

We conclude that facile reduction of P₃^BFe(NNH₂)⁺ to P₃^BFe(NNH₂), relative to that for P₃^{Si}Fe(NNH₂)⁺ and P₃^CFe(NNH₂)⁺, is one important factor in determining its comparative efficiency for N₂RR. As further elaborated below, long-lived P₃^EFe(NNH₂)⁺ intermediates can, via bimolecular PCET pathways, instead lead to unproductive HER. This HER activity, however, is dependent on both a long-lived P₃^EFe(NNH₂)⁺ intermediate, and the presence of a highly reactive PCET reagent, such as a P₃^EFe(NNH₂) species. We have previously postulated that P₃^EFe(NNH₂) formation is required for the release of the first equivalent of NH₃ and thus suggest that this species may be a crucial intermediate in both HER and N₂RR.^{4f,g,17}

Table 1. Calculated thermodynamic and kinetic parameters for P₃^EFe(NNH₂)⁺ → P₃^EFe(NNH₂)⁰

	P ₃ ^E Fe(NNH ₂) ⁺ + e [–] → P ₃ ^E Fe(NNH ₂) ⁰			
	E ⁰ (vs Fc ⁺⁰)	λ _{is,ET}	G* _{rel} ^b	k _{rel} ^b
E = B	–1.2 V	23	1.0	1
E = Si	–1.9 V	30	4.4	2x10 ^{–4}
E = C	–2.0 V	30	5.2	2x10 ^{–5}

^aEnergies are in kcal/mol, unless noted otherwise.

^bG*_{rel} values were calculated assuming a P₃^BFe(NNH₂)⁺ reduction barrier of 1.0 kcal/mol. k_{rel} ≡ exp[(G*_B–G*_E)/k_BT] where T = 195 K.

Calculated PCET Reactions

The differences in N–H bond strengths and relative rates of P₃^EFe(NNH₂)⁺ reduction, with corresponding implications for product selectivity, are further highlighted by calculating the thermodynamic and kinetic parameters for several PCET reactions of interest (Figure 4ABC). In

particular, comparative driving forces were calculated for unproductive bimolecular PCET reactions that generate H₂ between P₃^EFe(NNH₂)ⁿ⁺ (n = 0,1; E = B, Si, C) and P₃^EFe(NNH₂). Consistent with the calculated BDFE_{N-H} values (**Figure 3**), the P₃^{Si}Fe, and to a lesser extent the P₃^CFe, system shows a higher propensity to undergo PCET to liberate H₂ and the corresponding reduced Fe–NNH_y species. This is especially apparent in the reaction between two P₃^EFe(NNH₂)⁺ species, and in the cross-reaction between an P₃^EFe(NNH₂)⁺ cation and a neutral P₃^EFe(NNH₂) species.

In the former case, two P₃^EFe(NNH₂)⁺ (E = Si, C) species react in a very favorable step to form 0.5 equiv H₂ and P₃^EFe(NNH)⁺ (ΔG_{calc} = –17.5 kcal/mol and –16.5, respectively; **Figure 4A**). The reaction barrier is expected to be dominated in this case by the work required to bring two cationic species together in solution (~5 kcal/mol; see SI), highlighting the reactive nature of P₃^{C/Si}Fe(NNH₂)⁺. In contrast, P₃^BFe(NNH₂)⁺ shows a correspondingly uphill PCET reaction (ΔG_{calc} = +3.1 kcal/mol) in its self-combination to liberate H₂ and P₃^BFe(NNH)⁺,²³ P₃^BFe(NNH₂)⁺ is also much more readily reduced to P₃^BFe(NNH₂) (Table 1).

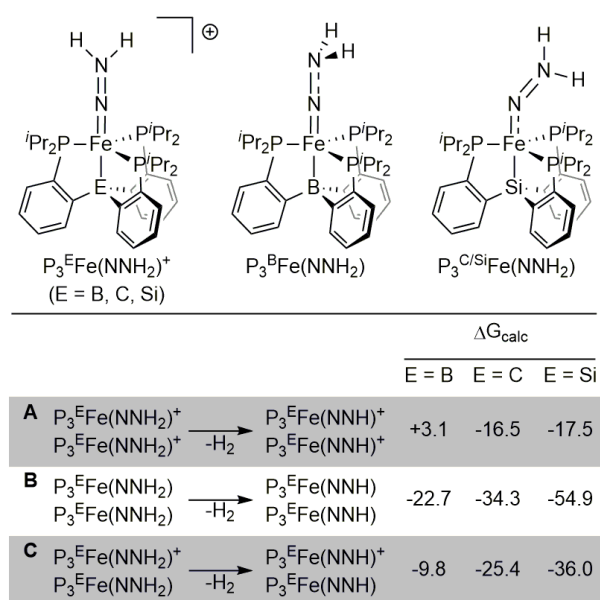


Figure 4. Calculated free energy changes (ΔG_{calc}; in kcal/mol; 195 K) for several putative PCET reactions that evolve H₂.

The bimolecular reaction between cationic P₃^EFe(NNH₂)⁺ with P₃^EFe(NNH₂) to produce H₂ and the corresponding P₃^EFe(NNH)⁺ and P₃^EFe(NNH) byproducts is predicted to be favorable for all three systems (**Figure 4C**). However, the P₃^{C/Si}Fe systems

proceed with far more driving force than the P₃^BFe system.

Favorable driving forces are also predicted for all three systems in self reactions of P₃^EFe(NNH₂) to produce H₂ and P₃^EFe(NNH), but again the P₃^{C/Si}Fe systems proceed with far more driving force (**Figure 4B**). While the bimolecular reaction of P₃^EFe(NNH₂) with itself is therefore a presumed source of H₂ for each system, in sum the P₃^{C/Si}Fe systems are more likely, under each of the considered bimolecular reactions, to liberate H₂, in accord with their efficiency for HER versus N₂RR relative to the P₃^BFe system.

Given that the reduction of P₃^{C/Si}Fe(NNH₂)⁺ is predicted to be comparatively slow, one might expect such a species to build-up as an intermediate. This possibility warrants future experimental studies aimed at in situ detection. At the present stage, we can suggest that a high (relative) concentration of P₃^{C/Si}Fe(NNH₂)⁺, and a high predicted propensity for HER via reaction of this species with either itself or P₃^{C/Si}Fe(NNH₂), leads to unproductive PCET steps that evolve H₂ as competitive with downstream N₂ reduction steps that lead to N₂RR. This is one important factor in determining selectivity.

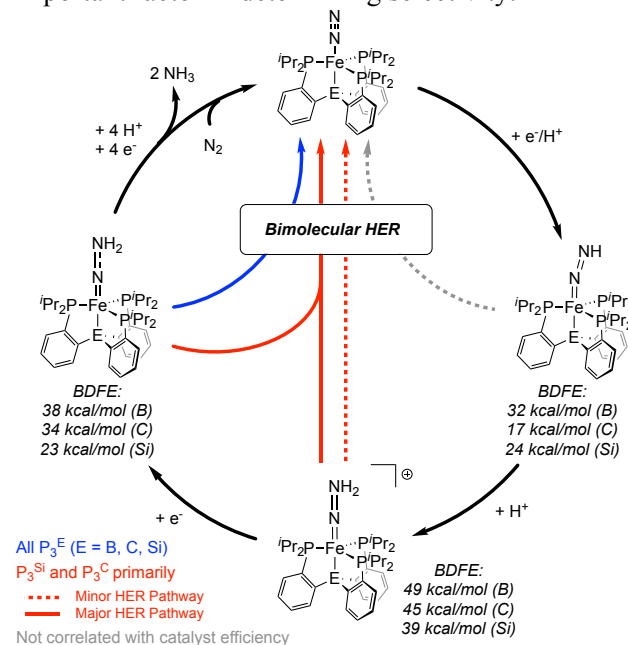


Figure 5. Overview of predicted bimolecular HER and N₂RR pathways for P₃^EFe(NNH_y) species and pertinent BDFE_{N-H} values.

Since the P₃^BFe(NNH₂)⁺ intermediate is predicted to have a lower propensity for H₂-liberating PCET reactivity, and is also predicted to be reduced much more rapidly, the reaction of two P₃^BFe(NNH₂) molecules is a more probable source of H₂ for this scaffold; the efficiency for N₂RR on P₃^BFe should therefore be related to the rate at which

$P_3^BFe(NNH_2)$ can be productively consumed (i.e., protonated to form a $P_3^BFe(NHNH_2)^+$ or $P_3^BFe(NNH_3)^+$). Mechanistic experiments to address these scenarios are ongoing. For example, a recent study has shown that $P_3^BFe(NNH_2)$ can be protonated by strong acid at low temperature to liberate $P_3^BFe(N)^+$ and NH_3 , presumably via $P_3^BFe(NNH_3)^+$.¹⁷

While the P_3^CFe scaffold provides a less definitive comparison, the calculated $BDFE_{N-H}$ values and H_2 -evolving PCET thermodynamics suggest that the dominant source of HER on the $P_3^{C/Si}Fe$ scaffolds may be the reaction between $Fe(NNH_2)$ and $Fe(NNH_2)^+$. The highly reducing nature of $P_3^CFe(NNH_2)^+$, as for the P_3^{Si} scaffold, suggests it should be comparatively long-lived, and thus more likely to undergo PCET with $P_3^CFe(NNH_2)$. The similarity between P_3^CFe and $P_3^{Si}Fe$ in their thermodynamics for the reaction between two $Fe(NNH_2)^+$ species (**Figure 4A**) does not correlate with their disparate % NH_3 efficiencies. Substantial differences in their predicted thermodynamics for the reaction between $Fe(NNH_2)$ and $Fe(NNH_2)^+$ (**Figure 4C**) are more in line with the observed trend. This type of bimolecular reactivity may be an important source of HER on the $P_3^{C/Si}Fe$ scaffolds (**Figure 5**).

Wiberg Bond Indices of $P_3^EFe(NxHy)$ Species

We next examine how each P_3^E auxiliary, and the corresponding $P_3^EFe(NNH_y)$ valence at iron, confers variability in bonding to, and the electronic structure of, the NNH_y ligand, as a means of further considering corresponding reactivity differences of $P_3^EFe(NNH_y)$ species.

Wiberg bond indices provide a means to examine how the localized bonding between various atoms, expressed as a bond index,²⁴ changes as a function of the NNH_y reduction state (i.e., NNH to NNH_2). We have suggested elsewhere that the relative flexibility of the P_3^B ligand, owing to a weak and dative $Fe \rightarrow B$ interaction, may allow for stabilization of $Fe-NNH_y$ intermediates where $Fe-N$ pi-bonding is accompanied by pyramidalization at the Fe center, and a corresponding lengthening of the $Fe-B$ distance.^{4a,17,25} The P_3^{Si} ligand is expected to give rise to a more shared, covalent $Fe-Si$ interaction, irrespective of the NNH_y reduction state, and the P_3^C system may be expected to fall in the middle of these extremes.^{4b}

Changes in the respective bond indices of these frameworks have been determined between pairs of $P_3^EFe(NNH)$ and $P_3^EFe(NNH_2)$ species ($E = B, C, Si$), related by formal addition of an H-atom to

the former. Interestingly, the N-H bond indices are essentially invariant across all complexes studied, indicating that differences in $BDFE_{N-H}$ are mostly dependent on the relative bonding through the $E-Fe-N-N$ manifold.²⁶ The most salient data, reproduced in **Figure 6**, are the total Wiberg bond indices for $Fe-N_\alpha$, $Fe-N_\beta$, $Fe-E$, $N-N$ and $N-H$. The total $Fe-N-N$ bond order, $\sum(Fe-N-N)$, is also provided, as is the net difference in the $\Delta BDFE_{N-H}$ value, for each pair on moving from $Fe(NNH)$ to $Fe(NNH_2)$.

As expected, the $Fe-E$ bond order weakens slightly from $Fe(NNH)$ to $Fe(NNH_2)$ for $E = B$, and stays constant for both Si and C. The respective change at $Fe-N_\alpha$ is also informative. For the B system, a significant increase is observed (1.6 to 1.9), reflecting a build-up in pi-bonding in $P_3^BFe(NNH_2)$, akin to low-spin (pseudotetrahedral) iron imides of the type $P_3^BFe(NR)$. For comparison, a previously characterized $P_3^BFe(NR)$ species ($R = 4-OMe-Ph$) is predicted to have an $Fe-N$ bond order of 1.8 (see SI).

By contrast, the $Fe-N_\alpha$ index for Si is sharply attenuated (from 1.6 to 1.2), reflecting a corresponding decrease in pi bonding. While this difference must partly reflect a less flexible $Fe-Si$ interaction, it also reflects the electronic structure resulting from an extra electron in the frontier orbitals of the 2E $\{Fe-Si\}^7$ system relative to 1A $\{Fe-B\}^6$. Interestingly, $P_3^BFe(NNH_2)$ is pyramidalized at N_β whereas N_β is planar for $P_3^{Si}Fe(NNH_2)$. This observation can again be rationalized by the assignment of a low-spin iron “imide-like” electronic structure to $\{Fe-B\}^6 P_3^BFe(NNH_2)$, but not for $\{Fe-Si\}^7 P_3^{Si}Fe(NNH_2)$, where substantial spin leaks onto the NNH_2 subunit (19% on $P_3^{Si}Fe(NNH_2)$). The C system provides an interesting further comparison, with spin leakage onto the NNH_2 unit falling between these two extremes (12% on $P_3^CFe(NNH_2)$). An increase in the $Fe-N_\alpha$ index occurs from $P_3^CFe(NNH)$ to $P_3^CFe(NNH_2)$ (1.2 to 1.4), but N_β is predicted to remain planar.

There also appears to be a strong trend between the degree of change in the total $Fe-N-N$ bond order ($\sum(Fe-N-N)$) and the $\Delta BDFE_{N-H}$. The B and C systems show little change in $\sum(Fe-N-N)$, with a corresponding significant increase in $BDFE_{N-H}$ from $Fe(NNH)$ to $Fe(NNH_2)$ (7.0 and 17.9 kcal/mol, respectively). However, the P_3^CFe system starts at a much weaker $BDFE_{N-H}$ of 17.3 kcal/mol for $P_3^CFe(NNH)$ (compared to 31.2 kcal/mol for P_3^BFe). This observation is consistent with their total $\sum(Fe-N-N)$ values (3.8 for B and 2.9 for C). Thus, the comparative stability of $P_3^CFe(NNH_2)$, with its much higher $BDFE_{N-H}$ relative that in $P_3^CFe(NNH)$,

appears to reflect a higher degree of instability in $P_3^E Fe(NNH)$ (relative to the same comparison for $E = B$). This idea is further supported by Wiberg bond indices of the $P_3^E Fe(N_2)$ species, which show a total bond order of 4.0 across the Fe–N–N unit for all three scaffolds (**Figure 6**).

In sharp contrast, the $P_3^{Si} Fe$ system has a relatively high $\Sigma(Fe-N-N)$ value in $P_3^{Si} Fe(NNH)$, but this value decreases dramatically in $P_3^{Si} Fe(NNH_2)$. There is correspondingly very little change in the $\Delta BDFE_{N-H}$, reflecting a comparatively very weak N–H bond in $P_3^{Si} Fe(NNH_2)$. The instability of $P_3^{Si} Fe(NNH_2)$, with an electronic structure that places substantial unpaired spin on NNH_2 owing to the $\{Fe-Si\}^7$ configuration, presumably contributes to the cathodically shifted reduction potential predicted for $P_3^{Si} Fe(NNH_2)^+$ relative to $P_3^B Fe(NNH_2)^+$, and also its propensity for facile PCET to liberate H_2 .

The $P_3^B Fe$ system is unique within this series in its ability to support a high total Fe–N–N bond order from $Fe(NNH)$ to $Fe(NNH_2)$, facilitating its trajectory along productive N_2RR .

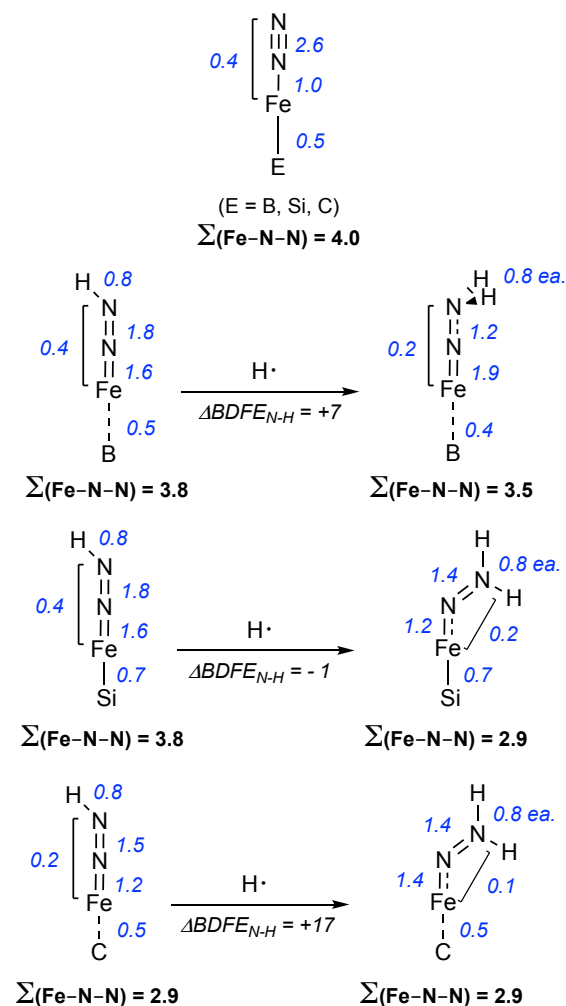


Figure 6. Selected total Wiberg bond indices for $P_3^E Fe(N_2)$, $P_3^E Fe(NNH)$ and $P_3^E Fe(NNH_2)$ species, along with the total Fe–N–N bond order, $\Sigma(Fe-N-N)$. $\Delta BDFE_{N-H}$ values are reported in kcal/mol.

Conclusion

Exploring the chemical basis for N_2RR versus HER selectivity for a molecular catalyst is important to future catalyst design. The DFT study described herein suggests that PCET reactions involving $P_3^E Fe(NNH_2)^{n+}$ species likely play an important role in the efficiency of N_2 -to- NH_3 conversion catalysis by $P_3^E Fe$ model systems. These calculations enable predictions qualitatively consistent with previous stoichiometric and catalytic experiments. The comparative stability of $P_3^E Fe(NNH_2)^{n+}$ intermediates, as predicted by calibrated $BDFE_{N-H}$ values and redox potentials, emerges as one of the important factors in determining selectivity for N_2RR versus HER in these systems. Corresponding Wiberg bond indices intimate P_3^B as an especially well-equipped ligand for supporting N_2RR at Fe, due to its high degree of flexibility and the valence electron count it confers to Fe in the reduced intermediate $P_3^B Fe(NNH_2)$. Our study suggests that increasing the rate at which an $P_3^E Fe(NNH_2)$ intermediate is productively consumed so as to avoid bimolecular HER, possibly via rapid PCET reagents, may be a promising route to increasing efficiency for NH_3 production.

Looking beyond these iron model systems, our study underscores the potential utility of DFT-predicted $BDFE_{N-H}$ determinations towards the rational design of catalysts for N_2RR . Intermediates with weak N–H bonds (e.g., $M(NNH)$ and $M(NNH_2)$) are highlighted as important sources of H_2 production via bimolecular PCET. Such a scenario is distinct from HER activity via more traditional metal-hydride intermediates.

ASSOCIATED CONTENT

Supporting Information.

The Supporting Information is available free of charge on the ACS Publications website.

Complete computational details, molecular geometries from the computations, additional computations and analysis (PDF)

AUTHOR INFORMATION

Corresponding Author

*jpeters@caltech.edu

Funding Sources

No competing financial interests have been declared.

ACKNOWLEDGMENT

This work was supported by the NIH (GM 070757) and the Gordon and Betty Moore Foundation, and the Extreme Science and Engineering Discovery Environment (XSEDE), which is supported by National Science Foundation grant number ACI-1053575. B.D.M. acknowledges the support of the NSF for a Graduate Fellowship (GRFP). We thank Matthew Chalkley for insightful input.

REFERENCE

¹ (a) Chatt, J.; Dilworth, J. R.; Richards, R. L. *Chem. Rev.* **1978**, *78*, 589-625. (b) Schrock, R. R. *Acc. Chem. Res.* **2005**, *38*, 955-962. (c) Nishibayashi, Y. *Inorg. Chem.* **2015**, *54*, 9234-9247. (d) van der Ham, C. J. M.; Koper, M. T. M.; Hetterscheid, D. G. H. *Chem. Soc. Rev.* **2014**, *43*, 5183-5191. (e) Shaver, M. P.; Fryzuk, M. D. *Adv. Synth. Catal.* **2003**, *345*, 1061-1076. (f) MacLeod, K. C.; Holland, P. L. *Nat. Chem.* **2013**, *5*, 559-565.

² (a) Howard, J. B.; Rees, D. C. *Proc. Nat. Acad. Sci.* **2006**, *103*, 17088-17093. (b) Howard, J. B.; Rees, D. C. *Chem. Rev.* **1996**, *96*, 2965-2982.

³ Hoffman, B. M.; Lukoyanov, D.; Yang, Z.-Y.; Dean, D. R.; Seefeldt, L. C. *Chem. Rev.* **2014**, *114*, 4041-4062.

⁴ For pertinent Fe systems: (a) Anderson, J. S.; Rittle, J.; Peters, J. C. *Nature* **2013**, *501*, 84-87. (b) Creutz, S. E.; Peters, J. C. *J. Am. Chem. Soc.* **2014**, *136*, 1105-1115. (c) Ung, G.; Peters, J. C. *Angew. Chem., Int. Ed.* **2015**, *54*, 532-535. (d) Del Castillo, T. J.; Thompson, N. B.; Peters, J. C. *J. Am. Chem. Soc.* **2016**, *138*, 5341-5350. (e) Chalkley, M. J.; Del Castillo, T. J.; Matson, B. D.; Roddy, J. P.; Peters, J. C. *ACS Central Science* **2017**, *3*, 217-223. (f) Anderson, J. S.; Cutsail, G. E.; Rittle, J.; Connor, B. A.; Gunderson, W. A.; Zhang, L.; Hoffman, B. M.; Peters, J. C. *J. Am. Chem. Soc.* **2015**, *137*, 7803-7809. (g) Rittle, J.; Peters, J. C. *J. Am. Chem. Soc.* **2016**, *138*, 4243-4248. (h) Rittle, J.; Peters, J. C. *J. Am. Chem. Soc.* **2017**, *139*, 3161-3170.

⁵ For Mo systems: (a) Kuriyama, S.; Arashiba, K.; Nakajima, K.; Matsuo, Y.; Tanaka, H.; Ishii, K.; Yoshizawa, K.; Nishibayashi, Y. *Nat. Commun.* **2016**, *7*, 12181. (b) Yandulov, D. V.; Schrock, R. R. *Science* **2003**, *301*, 76-78. (c) Arashiba, K.; Miyake, Y.; Nishibayashi, Y. *Nat. Chem.* **2011**, *3*, 120-125. (d) Kuriyama, S.; Arashiba, K.; Nakajima, K.; Tanaka, H.; Kamaru, N.; Yoshizawa, K.; Nishibayashi, Y. *J. Am. Chem. Soc.* **2014**, *136*, 9719-9731. (e) Arashiba, K.; Kinoshita, E.; Kuriyama, S.; Eizawa, A.; Nakajima, K.; Tanaka, H.; Yoshizawa, K.; Nishibayashi, Y. *J. Am. Chem. Soc.* **2015**, *137*, 5666-5669.

⁶ For Co systems: (a) Del Castillo, T. J.; Thompson, N. B.; Suess, D. L. M.; Ung, G.; Peters, J. C. *Inorg.*

Chem. **2015**, *54*, 9256-9262. (b) Kuriyama, S.; Arashiba, K.; Tanaka, H.; Y. Matsuo, Y.; Nakajima, K.; Yoshizawa, K.; Nishibayashi, Y. *Angew. Chem. Int. Ed.* **2016**, *55*, 14291-14295.

⁷ (a) Reiher, M.; Le Guennic, B.; Kirchner, B. *Inorg. Chem.* **2005**, *44*, 9640-9642. (c) Studt, F.; Tucek, F. *Angew. Chem. Int. Ed.* **2005**, *44*, 5639-5642. (d) Studt, F.; Tucek, F. *J. Comput. Chem.* **2006**, *27*, 1278-1291. (e) Ujjal Gogoi, U.; Kanti Guha, A.; Phukan, A. K. *Chem. Eur. J.* **2013**, *19*, 11077-11089.

⁸ Side-by-side comparisons of catalytic N₂RR by P₃^EFe (E = B, C, and Si) using potassium graphite (KC₈) and [(Et₂O)₂H][BAR^F₄] (HBAR^F₄, BAR^F₄ = tetrakis-(3,5-bis(trifluoromethyl)phenyl)borate) have revealed P₃^BFe to be the most efficient catalyst, with reported efficiencies up to 37%. N₂RR catalysis by P₃^CFe or P₃^{Si}Fe is less efficient under these conditions, with reported efficiencies of 33% and 4%, respectively. Studies focused on HER catalysis have shown P₃^{Si}Fe(N₂)⁻ (88% per H⁺) to be significantly more efficient than P₃^BFe(N₂)⁻ (40% per H⁺) under analogous conditions. See 4d.

⁹ In this study, we do not distinguish between the terms H-atom transfer (HAT) vs PCET. For consistency, we refer to PCET throughout. For discussion of terminology see: (a) Warren, J. J.; Tronic, T. A.; Mayer, J. M. *Chem. Rev.* **2010**, *110*, 6961-7001. (b) Hammes-Schiffer, S. *J. Am. Chem. Soc.* **2015**, *137*, 8860-8871.

¹⁰ Grimme, S.; Antony, J.; Ehrlich, S.; Krieg, H. *J. Chem. Phys.* **2010**, *132*, 154104.

¹¹ Tao, J. M.; Perdew, J. P.; Staroverov, V. N.; Scuseria, G. E. *Phys. Rev. Lett.* **2003**, *91*, 146401.

¹² Weigend, F.; Ahlrichs, R. *Phys. Chem. Chem. Phys.* **2005**, *7*, 3297-3305.

¹³ Valiev, M.; Bylaska, E. J.; Govind, N.; Kowalski, K.; Straatsma, T. P.; Van Dam, H. J. J.; Wang, D.; Nieplocha, J.; Apra, E.; Windus, T. L.; de Jong, W. A. *Comput. Phys. Commun.* **2010**, *181*, 1477-1489.

¹⁴ Neese, F. *Wiley Interdiscip. Rev. Comput. Mol. Sci.* **2012**, *2*, 73-78.

¹⁵ (a) Klamt, A.; Schüürmann, G. *J. Chem. Soc. Perkin Trans. 2.* **1993**, *2*, 799-805. (b) Marten, B.; Kim, K.; Cortis, C.; Friesner, R. A.; Murphy, R. B.; Ringnalda, M. N.; Sitkoff, D.; Honig, B. *J. Phys. Chem.* **1996**, *100*, 11775-11788.

¹⁶ (a) Ribeiro, R. F.; Marenich, A. V.; Cramer, C. J.; Truhlar, D. G. *J. Phys. Chem. B* **2011**, *115*, 14556-14562. (b) Wang, T.; Brudvig, G.; Batista, V. S. *J. Chem. Theory Comput.* **2010**, *6*, 755-760. (c) Marten, B.; Kim, K.; Cortis, C.; Friesner, R. A.; Murphy, R. B.; Ringnalda, M. N.; Sitkoff, D.; Honig, B. *J. Phys. Chem.* **1996**, *100*, 11775-11788.

¹⁷ Thompson, N.B.; Green, M. T.; Peters, J.C. *J. Am. Chem. Soc.*, **2017**, *139*, 16105-16108.

¹⁸ Marcus, R. A. *J. Chem. Phys.* **1956**, *24*, 966-978.

¹⁹ (a) Dempsey, J. L.; Brunschwig, B. S.; Winkler, J. R.; Gray, H. B. *Acc. Chem. Res.* **2009**, *42*, 1995-2004. (b) Lewandowska-Andralojc, A.; Baine, T.; Zhao, X.; Muckerman, J. T.; Fujita, E.; Polyansky, D. E. *Inorg.*

1
2 *Chem.* **2015**, *54*, 4310–4321. (c) Yang, J. Y.; Smith, S. E.;
3 Liu, T.; Dougherty, W. G.; Hoffert, W. A.; Kassel, W. S.;
4 DuBois, M. R.; DuBois, D. L.; Bullock, R. M. *J. Am.*
5 *Chem. Soc.* **2013**, *135*, 9700–9712.

6 ²⁰ Brookhart, M.; Grant, B.; Volpe Jr., A. F.
7 *Organometallics* **1992**, *11*, 3920–3922.

8 ²¹ Fajardo, J.; Peters, J. C. *J. Am. Chem. Soc.* **2017**, *139*,
9 16105–16108.

10 ²² We have previously reported bond dissociation
11 enthalpies (BDE_{N-H}) for P₃^BFe(NNH) and P₃^BFe(NNH₂)
12 (see ref 4e). Here we reported BDFE_{N-H} values as they
13 have more theoretical justification in the absence of
14 experimental knowledge of the entropy change associated
15 with H· loss.

²³ While this discussion may seem at odds with the
enhanced stability of P₃^{Si}Fe(NNH₂)⁺ relative to
P₃^BFe(NNH₂)⁺, other factors are presumably responsible
in solution, such as the more facile reduction of
P₃^BFe(NNH₂)⁺ relative to P₃^{Si}Fe(NNH₂)⁺.

²⁴ Wiberg, K. B. *Tetrahedron*, **1968**, *24*, 1083-1096.

²⁵ Moret, M.-E.; Peters, J. C. *J. Am. Chem. Soc.*, **2011**,
133, 18118-18121.

²⁶ Similarly, the C₂H₅ radical is predicted to have a very
low BDFE_{C-H} (34 kcal/mol) when compared to C₂H₄ (100
kcal/mol), but the Wiberg bond indices for their
respective C–H bonds do not change appreciably (See SI).

TOC Graphic

